Saudi Journal of Radiology
December 2025, 61-78
Proceeding of the 16th Annual Meeting of Radiology Society of Saudi Arabia (RSSA)
Original Article

IMAGING CORRELATION OF MENINGIOMA BY CT AND MRI AMONG SAUDI PATIENTS

Nouf Alqahtani[1], Mohamed Bayomi[1], Basim Almutairi[1], Sarah Alqahtani[2], Shahad Alasmari[1], Eman Alqahtani[1], Abdu Alnaji[1], Juman Alghamdi[1]

[1]Department of Medical Imaging, King Saud Medical City, Riyadh, Saudi Arabia

[2]Department of Anatomical Pathology, College of Medicine, King Saud University Medical City, Riyadh, Saudi Arabia

Corresponding Author

Nouf Alqahtani, Department of Medical Imaging, King Saud Medical City, Riyadh, Saudi Arabia
Email:alqahtani.inouf@gmail.com

eISSN: 1658-8959

ABSTRACT

Background: Meningiomas are the most common primary intracranial tumors in adults, and accurate preoperative imaging is essential for diagnosis, surgical planning, and risk assessment. Computed Tomography (CT) and Magnetic Resonance Imaging (MRI) play complementary roles. Based on our review, no prior research in Saudi Arabia has statistically examined the correlation between CT and MRI findings, specifically tumor consistency, border definition, and signal homogeneity within the same cohort. This study aimed to evaluate demographic patterns and imaging characteristics of intracranial meningiomas in Saudi patients.

Methods and Materials: A cross-sectional study was conducted on 100 patients diagnosed with intracranial meningioma at King Saud Medical City from January 2022 to January 2025. Data were collected through a web-based form and imaging reports. Statistical analysis, including chi-square tests, Cohen's Kappa, and 95% confidence intervals (CIs) were calculated. The study assessed tumor location, morphology, enhancement patterns, peritumoral edema, and vascular involvement.

Results: Most patients were female (72%), with peak prevalence in the 51–60-year age group (28%). CT revealed heterogeneous tumor density (56%), calcifications (47%), and hyperostosis (26%). MRI showed 75% of lesions were hypointense on T1-weighted images, 40% were hyperintense on T2-weighted images, and 47% were isointense on T2-weighted FLAIR images. Dural tail appeared in 44%. Significant correlations were found between CT and MRI in tumor consistency ($p = 0.001$), borders ($p < 0.001$), and

homogeneity (p = 0.002). Cohen's Kappa showed fair agreement between the two modalities in these features. Diffusion restriction was associated with peritumoral edema (p = 0.002), and calcification with bone changes on CT (p < 0.001).

Conclusion: This study provides region-specific evidence of CT–MRI correlations in meningiomas among Saudi patients. CT is essential for detecting calcification and bone involvement, whereas MRI better characterizes soft tissue features and peritumoral changes. Combined , both modalities enhance diagnostic confidence and preoperative planning.

Keywords: Computed Tomography, Magnetic Resonance Imaging, Meningioma, Imaging Correlation, Preoperative Planning

1. INTRODUCTION

Meningiomas are the most common brain tumors in adults, presenting a diagnostic challenge. The advent of imaging has facilitated increased appreciation of the extraordinary multiplicity in the pattern of growth along the intracranial convexities and the base of the skull. [1] Complete tumor removal often provides good outcomes for the patients. However, few reports exist on the imaging-controlled results of meningiomas. The lack of accurate preoperative differential diagnosis might necessitate unnecessary increased morbidity and mortality due to tumor biopsy, incomplete tumor removal, and postoperative adjunct treatment for the patients. [1, 2] While international studies on meningiomas are abundant, previous Saudi studies have provided valuable data but were often limited by focusing on selected imaging characteristics, relying on small sample sizes, or lacking comprehensive CT–MRI statistical correlation. By addressing these limitations, the present study aims to comprehensively evaluate intracranial meningiomas among Saudi patients, including demographic characteristics and imaging features on CT and MRI, and to statistically examine correlations between CT and MRI findings particularly tumor consistency, border definition, and signal homogeneity in order to enhance diagnostic confidence and support preoperative planning.

1.1 Background of Meningioma

The classification of meningiomas under tumors of mesenchymal origin affirms their unique nature and origin. The distinguishing feature of meningiomas is that they arise from the meninges. [3] Meningiomas represent 35.3% of all primary

intracranial tumors, making them the most common primary intracranial tumors in adults.

Statistical data show that females suffer from meningioma at more than twice the frequency observed in males, and this frequency increases with age, particularly in the sixth and seventh decades of life. [1, 4]

It is known that meningioma is a slow-growing benign tumor and that, in the overwhelming majority of cases, the standard treatment consists of total removal of the tumor. [1, 4] However, in some cases, total removal is not possible due to the close proximity of fundamental brain structures, which might lead to great operational risk being assumed. In those cases, some treatment methods make a distinction between the resectable and unresectable tumors. [1, 4]

1.2 Significance of Imaging in Meningioma Diagnosis

Computed tomography (CT) provides diagnostic and informative data, which serves to evaluate the position of the lesions in the cranial cavity, the character of surrounding areas, and the relationships of the neoplasm with surrounding bony structures (Figure 1). [4, 5]

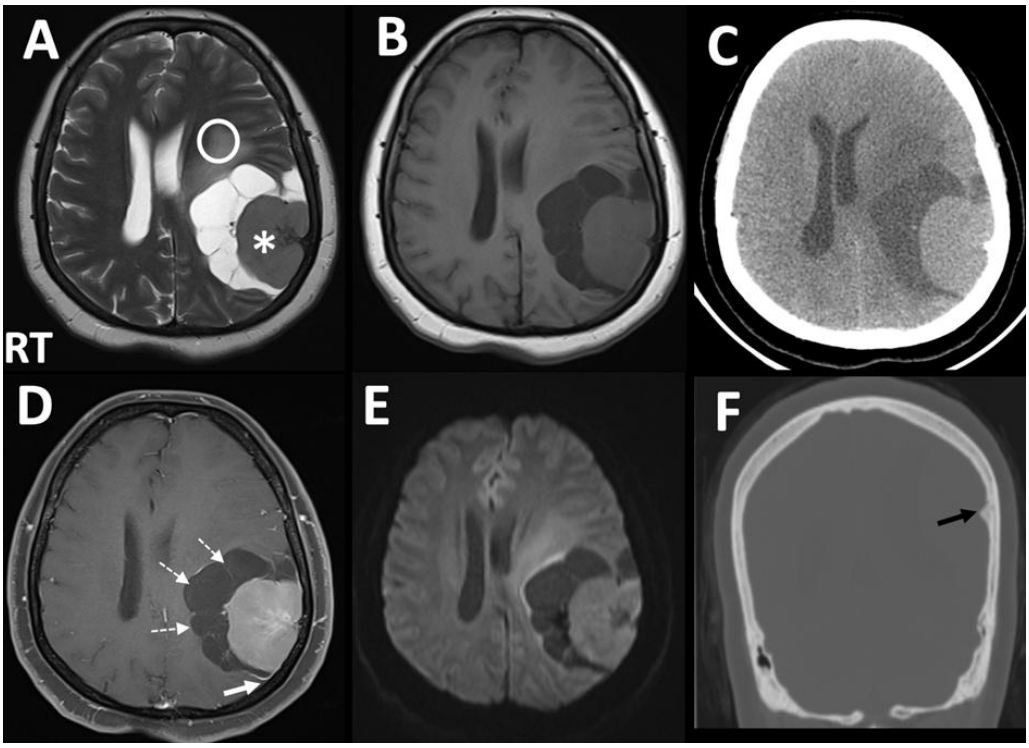

Figure 1. MR and CT images of a large left parietal convexity dural-based meningioma. The lesion demonstrates a solid component (asterisks) with isointense signal on both T2- and T1-weighted images (A, B), slight hyperdensity on non- contrast CT (C), and avid enhancement on axial post-

contrast T1-weighted images (D). No diffusion restriction is seen on diffusion-weighted imaging (E). The mass exerts a mass effect on adjacent structures, including compression of the left lateral ventricle, and is associated with moderate perilesional vasogenic edema (white circle). Cystic changes are observed around the lesion (dashed arrow), and an enhancing dural tail is evident (white arrow). A residual bony stump is visible on coronal CT in the bone window setting (black arrow)

The CT technique is the method of choice for the purpose of preoperative skull bone examination. With the help of angiography, it is possible to evaluate tumor blood supply more precisely, which is important in the case of planning surgical intervention. [5] Technology evolving diagnostic imaging studies, including magnetic resonance imaging (MRI), provides an extensive amount of information about these tumors and about which one can make reasonable assumptions concerning the nature and properties, specifically in tumors with well-defined characteristics (Figure 2). [1, 6]

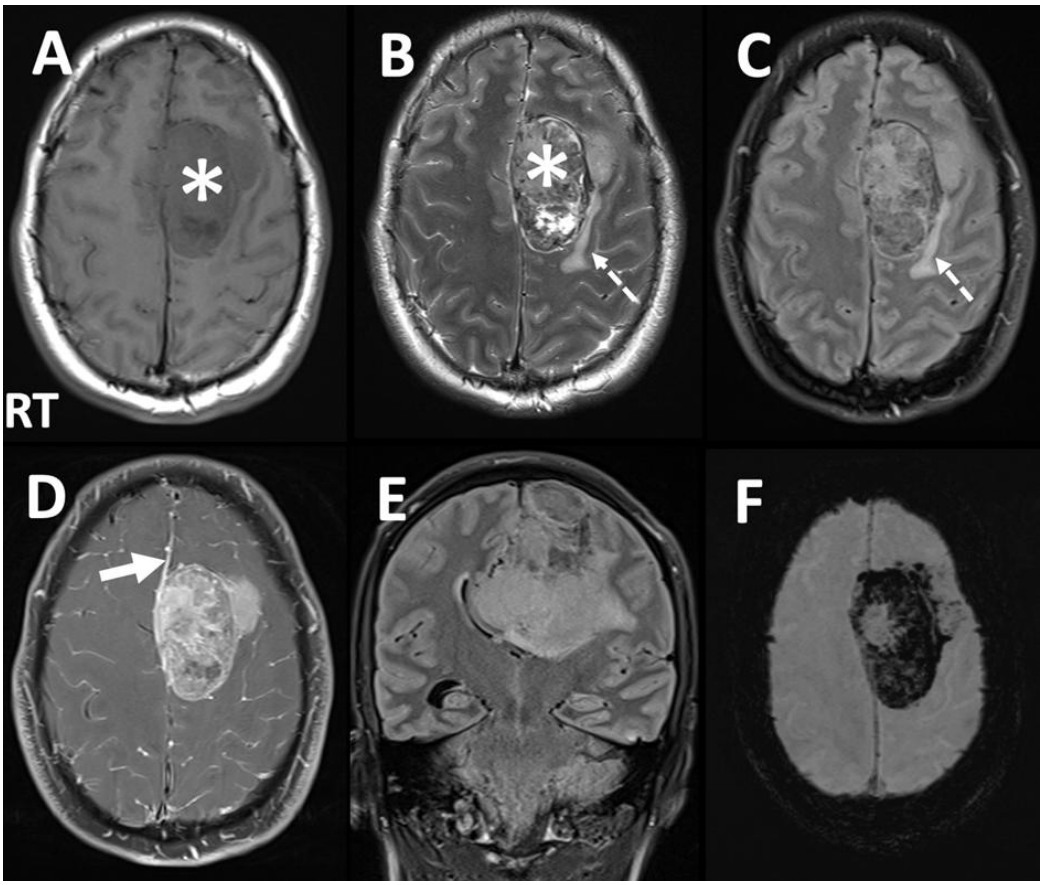

Figure 2. MR images demonstrate left parasagittal extra-axial, dural-based meningioma. The lesion appears predominantly hypointense on T1-weighted

images (A) and shows heterogeneous isointense signal on T2-weighted images (asterisks) (B) and T2-FLAIR images (C) with areas of cystic degeneration and signal voids suggestive of calcification or intralesional vascularity. Post-contrast T1-weighted images (D) and coronal T2 -FLAIR images (E) reveal intense enhancement with an enhancing dural tail (white arrow). Susceptibility-weighted imaging (F) shows signal loss consistent with calcification or hemorrhage. There is associated perilesional vasogenic edema (dashed arrow), mass effect on the ipsilateral lateral ventricle, and midline shift to the right (E).

In the opinion of the majority, the most important diagnostic task in the event of meningioma is to differentiate this neoplasm from other lesions situated in the cranial cavity, and in particular, from diffuse meningeal processes, focal inflammatory changes, and metastatic neoplasms. [4] Other important aspects include the evaluation of the relationship of the tumor with its craniocerebral surroundings, planning neurosurgical intervention, and finally, assessment of the degree of metabolic, circulatory, and vasomotor disturbances in the tumor and peritumoral area, which support therapeutic monitoring. [4] Although histopathology remains the gold standard for final confirmation and grading of meningiomas; imaging provides indispensable information for preoperative evaluation and surgical decision-making.

2. MATERIALS AND METHODS

2.1 Study Design and Population

This cross-sectional retrospective study employed a consecutive sampling technique and included 100 patients who met the eligibility criteria. Inclusion criteria were: (i) a radiologically confirmed first diagnosis of intracranial meningioma and (ii) Saudi nationality. Cases were excluded if they involved extracranial meningiomas, prior intracranial surgery, incomplete imaging studies (availability of only CT or only MRI without both modalities), or if image quality was insufficient to allow a confident diagnosis. All eligible patients during the study period were included after applying these criteria. Between January 2022 and January 2025, participants were identified from King Saud Medical City (KSMC) in Riyadh, Saudi Arabia.

2.2 Data Collection

Data collection was conducted using a web-based data form, completed by a neuroradiology consultant and neuroradiology fellow. MRI and CT images, along

with radiological reports, were reviewed to assess meningioma characteristics, imaging features, and associated findings.

2.3 CT Protocol

All CT examinations were performed either on a Siemens SOMATOM Definition Flash 64-slice scanner or a Siemens Discovery Dual Energy 256-slice scanner. Imaging parameters included a tube voltage of 120 kVp, a tube current of 220 mA, and a slice thickness ranging from 3.75 mm to 5 mm, with image reconstruction at 1.25 mm intervals. The field of view (FOV) was adjusted between 22 and 24 cm, depending on patient size and anatomical coverage. The pitch value ranged from 0.5 to 0.9 to optimize spatial resolution while minimizing radiation dose.

For contrast-enhanced studies, the contrast agents used were Omnipaque (iohexol) in varying concentrations or Visipaque 320(iodixanol), with the dosage adjusted according to patient weight.

2.4 MRI Protocol

MRI examinations were performed using Siemens MAGNETOM Skyra 3.0 Tesla, GE Optima 1.5 Tesla, or GE SIGNA Artist 1.5 Tesla. A standardized imaging protocol was applied across all machines to ensure consistency in image acquisition and diagnostic comparability. Pre-contrast sequences included sagittal T1-weighted images, axial T2-weighted images, axial T2 FLAIR (Fluid-Attenuated Inversion Recovery) images, axial diffusion-weighted images (DWI), axial gradient echo (GRE) or susceptibility-weighted images (SWI), and coronal T2-weighted images. Following the administration of gadobutrol (Gadovist®) at a dose of 0.1 mmol/kg, post-contrast sequences were acquired, including axial T1-weighted fat-saturated, axial post-contrast T2 FLAIR fat-saturated, and sagittal post-contrast T1-weighted images. All sequences were acquired with a slice thickness of 4 mm to 5 mm and an inter-slice gap of 0.5 mm to 2.5 mm. The field of view (FOV) ranged from 22 to 24 cm, depending on patient size and anatomical coverage.

2.5 Imaging Evaluation

Tumor characteristics were assessed using standardized visual radiologic criteria. Consistency was categorized as solid when the lesion demonstrated uniform attenuation or signal intensity without cystic or necrotic changes, and as mixed when such components were present. Borders were classified as well defined if

sharply demarcated from adjacent parenchyma, poorly defined if indistinct, or mixed when both patterns coexisted. Signal homogeneity was described as homogeneous when the lesion appeared uniform and heterogeneous when attenuation or signal intensity varied. Enhancement intensity on CT and MRI was graded as mild, moderate, or intense based on the radiologist's visual impression relative to gray and white matter.

Each reader independently reviewed assigned cases; in situations of uncertainty, the case was re-evaluated in consensus under the consultant's supervision. Clinical information was available at the time of image review, and readers were not blinded to clinical data. Inter-observer variability analysis was not performed, as cases were divided between readers rather than double-read.

2.6 Data Sources and Statistical Analysis

Data sources included hospital records, the radiology information system (RIS), picture archiving and communication system (PACS), and clinical charts. Data were processed and analyzed using SPSS version 22, Microsoft Excel, and Power BI for statistical reporting and visualization. Descriptive statistics included frequencies for categorical variables. Ninety-five percent confidence intervals (95% CIs) were calculated for major proportions to provide precision of estimates. Associations between categorical imaging features were assessed using the Pearson chi-square test. Cohen's Kappa was used to assess agreement between CT and MRI findings. All data were handled confidentially and stored securely for research purposes.

3. RESULTS

A total of 100 patients were included in the study, comprising 72 females (72%, 95% CI: 62.5–79.9) and 28 males (28%, 95% CI: 20.1–37.5). Age distribution was as follows: 5 patients were under 30 years (5%, 95% CI: 2.2–11.2), 8 were between 30 and 40 years (8%, 95% CI: 4.1–15.0), 25 were between 41 and 50 years (25%, 95% CI: 17.5–34.3) , 28 were between 51 and 60 years (28%, 95% CI: 20.1–37.5), 19 were between 61 and 70 years (19%, 95% CI: 12.5–27.8), and 15 were above 71 years (15%, 95% CI: 9.3–23.3). All collected variables are detailed in the text, while selected demographic and imaging features are summarized in Table 1.

The most common presenting symptoms included non-specific symptoms in 51 patients (51%, 95% CI: 41.3–60.6), side weakness in 10 (10%, 95% CI: 5.5–17.4), seizures in 9 (9%, 95% CI: 4.8–16.2), and headache in 8 (8%, 95% CI: 4.1–15.0). Combined symptom presentations were observed in 16 patients with

headache and other symptoms (16%, 95% CI: 10.1–24.4), 2 with headache and seizures (2%, 95% CI: 0.6–7.0), 2 with side weakness and other symptoms (2%, 95% CI: 0.6–7.0), 1 with headache and side weakness (1%, 95% CI: 0.2–5.4), and 1 with seizures and other symptoms (1%, 95% CI: 0.2–5.4).

Table 1. Demographic Characteristics and Key Imaging Features in 100 Patients with Intracranial Meningioma.

Category	Feature	N (%)
Gender	Female	72 (72%)
	Male	28 (28%)
MRI T1	Hyperintense	6 (6%)
	Hypointense	75 (75%)
	Isointense	17 (17%)
	Heterogeneous	2 (2%)
MRI T2	Hyperintense	40 (40%)
	Hypointense	16 (16%)
	Isointense	28 (28%)
	Heterogeneous	16 (16%)
MRI FLAIR	Hyperintense	38 (38%)
	Hypointense	16 (16%)
	Isointense	46 (46%)
MRI DWI	Yes	22 (22%)
	No	78 (78%)
MRI Dural Tail	Yes	44 (44%)

	No	56 (56%)
CT Appearance	Hypodense	6 (6%)
	Isodense	21 (21%)
	Heterogeneous	73 (73%)
CT Calcification	Yes	47 (47%)
	No	53 (53%)
CT Bone Changes	Hyperostosis	26 (26%)
	Erosion	15 (15%)
	None	59 (59%)
MRI Consistency	Solid	92 (92%)
	Mixed	8 (8%)
MRI Tumor Borders	Well–defined	82 (82%)
	Poorly defined	7 (7%)
	Mixed	11 (11%)
MRI Homogeneity	Homogeneous	55 (55%)
	Heterogeneous	45 (45%)
CT Consistency	Solid	87 (87%)
	Mixed	13 (13%)
CT Tumor Borders	Well-defined	73 (73%)
	Poorly defined	12 (12%)
	Mixed	15 (15%)
CT Homogeneity	Homogeneous	44 (44%)

Heterogeneous	56 (56%)

Tumor locations were most frequently observed in the convexity (45%, 95% CI: 35.6–54.8), followed by (18%, 95% CI: 11.7–26.7), cerebellopontine angle (CPA) 8%, 95% CI: 4.1–15.0), sellar/suprasellar region (8%, 95% CI: 4.1–15.0), sphenoid wing (3%, 95% CI: 1.0–8.5), tentorium (4%, 95% CI: 1.6–9.8), dorsum sellae (1%, 95% CI: 0.2–5.4), planum sphenoidale (4%, 95% CI: 1.6–9.8), olfactory groove (4%, 95% CI: 1.6–9.8), intraventricular region (1%, 95% CI: 0.2–5.4), and other sites (4%, 95% CI: 1.6–9.8).

Evaluation of tumor proximity to adjacent neuroanatomical structures showed involvement of the superior sagittal sinuses and transverse sinuses in 23% (95% CI: 15.8–32.2), cranial nerves in 9% (95% CI: 4.8–16.2), brainstem in 8% (95% CI: 4.1–15.0), optic nerve in 6% (95% CI: 2.8–12.5), cavernous sinus in 4% (95% CI: 1.6–9.8), pituitary gland in 2% (95% CI: 0.6–7.0), suprasellar region in 2% (95% CI: 0.6–7.0), and foramen magnum in 1% (95% CI: 0.2–5.4). In 45% of patients (95% CI: 35.6–54.8), no proximity to critical structures was identified.

Most tumors were rounded in shape 63% (95% CI: 53.2–71.8), irregular in 24% (95% CI: 16.7–33.2), and lobulated in 13% (95% CI: 7.8–21.0). Associated findings included mass effect in 42 patients (42%, 95% CI: 32.8–51.8), hydrocephalus without midline shift in 17 (17%, 95% CI: 10.9–25.5), mass effect with midline shift in 20 (20%, 95% CI: 13.3–28.9), mass effect with both midline shift and hydrocephalus in 14 (14%, 95% CI: 8.5–22.1), and mass effect with hydrocephalus in 3 (3%, 95% CI: 1.0–8.5). No associated findings were present in 21 patients (21%, 95% CI: 14.2–30.0). Regarding vascular relationships, adjacent vessel abutment in 35% (95% CI: 26.4–44.7), vascular narrowing in 17% (95% CI: 10.9–25.5), vascular invasion in 4% (95% CI: 1.6–9.8), and feeding artery in 1% (95% CI: 0.2–5.4). No vascular involvement was observed in 43% (95% CI: 33.7–52.8).

3.1 CT Imaging Characteristics

CT findings demonstrated homogeneous density in 44 cases (44%, 95% CI: 34.7–53.8) and heterogeneous density in 56 cases (56%, 95% CI: 46.2–65.3). A total of 62 (62%) patients did not receive contrast, either because it was deemed unnecessary or due to contraindications or preparation-related limitations. Among the 38 contrast-enhanced scans, enhancement was homogeneous in 16 cases (42.1%, 95% CI: 27.9–57.8) and heterogeneous in 22 cases (57.9%, 95% CI: 42.2–72.1). The degree of enhancement in this group was mild in 24 (63.2%, 95% CI: 47.3–76.7), moderate in 10 (26.3%, 95% CI: 14.7–42.0), and intense in

4 (10.5%, 95% CI: 4.2–24.1). Tumor consistency was reported as solid in 87 patients (87%, 95% CI: 79.0–92.2) and mixed in 13 patients (13%, 95% CI: 7.8–21.0). Tumor borders were well-defined in 73 cases (73%, 95% CI: 63.6–80.7), poorly defined in 12 cases (12%, 95% CI: 7.0–19.8), and mixed in 15 cases (15%, 95% CI: 9.3–23.3).

Bone changes included hyperostosis in 26 patients (26%, 95% CI: 18.4–35.4), erosion in 15 patients (15%, 95% CI: 9.3–23.3), and no bone changes in 59 patients (59%, 95% CI: 49.2–68.1). Calcification was observed in 47 patients (47%, 95% CI: 37.5–56.7), while 53 patients (53%, 95% CI: 43.3–62.5) showed no calcification.

Overall CT appearance was reported as heterogeneous in 73 patients (73%, 95% CI: 63.6–80.7), isodense in 21 patients (21%, 95% CI: 14.2–30.0), and hypodense in 6 patients (6%, 95% CI: 2.8–12.5).

3.2 MR Imaging Characteristics

MRI findings revealed solid tumor consistency in 92 patients (92%, 95% CI: 85.0–95.9) and mixed consistency in 8 patients (8%, 95% CI: 4.1–15.0).Tumor borders were well-defined in 82 cases (82%, 95% CI: 73.3–88.3), poorly defined in 7 (7%, 95% CI: 3.4–13.7), and mixed in 11 (11%, 95% CI: 6.3–18.6). Signal homogeneity was homogeneous in 55 patients (55%, 95% CI: 45.2–64.4) and heterogeneous in 45 (45%, 95% CI: 35.6–54.8). Among the 99 contrast-enhanced scans, enhancement was homogeneous in 58 (58.6%, 95% CI: 48.7–67.8) and heterogeneous in 41 (41.4%, 95% CI: 32.2–51.3), while 1 patient (1%, 95% CI: 0.2–5.4) did not receive contrast. The degree of enhancement was mild in 18 patients (18%, 95% CI: 11.7–26.7), moderate in 34 (34%, 95% CI: 25.5–43.7), intense in 34 (34%, 95% CI: 25.5–43.7), and absent in 13 (13%, 95% CI: 7.8–21.0). The dural tail sign was present in 44 patients (44%, 95% CI: 34.7–53.8) and absent in 56 (56%, 95% CI: 46.2–65.3). On T1-weighted images, signal intensity was hypointense to gray matter in 75 lesions (75%, 95% CI: 65.7–82.5), isointense in 17 (17%, 95% CI: 10.9–25.5), hyperintense in 6 (6%, 95% CI: 2.8–12.5), and heterogeneous in 2 (2%, 95% CI: 0.6–7.0). On T2-weighted images, signal intensity was hyperintense in 40 lesions (40%, 95% CI: 30.9–49.8), isointense in 28 (28%, 95% CI: 20.1–37.5), hypointense in 16 (16%, 95% CI: 10.1–24.4), and heterogeneous in 16 (16%, 95% CI: 10.1–24.4). On FLAIR sequences, 46 lesions (46%, 95% CI: 36.6–55.7) were isointense, 38 (38%, 95% CI: 29.1–47.8) were hyperintense, and 16 (16%, 95% CI: 10.1–24.4) were hypointense relative to gray matter. Restricted diffusion was observed in 22 patients (22%, 95% CI: 15.0–31.1), while 78 patients (78%, 95% CI: 68.9–85.0) showed no restriction. Peritumoral edema was present in 36 patients (36%, 95%

CI: 27.3–45.8), while 64 patients (64%, 95% CI: 54.2–72.7) showed no edema. Among the 36 patients with edema, 19 (52.8%, 95% CI: 36.5–68.6) had mild, 13 (36.1%, 95% CI: 21.5–53.8) had moderate, and 4 (11.1%, 95% CI: 4.4–25.4) had severe edema.

3.3 Statistical Correlation and Interpretation

Chi-square analysis revealed several statistically significant associations between CT and MR imaging features. A significant correlation was observed between CT and MRI consistency ($\chi^2 = 10.526$, $p = 0.001$), tumor borders ($\chi^2 = 30.483$, $p < 0.001$), and signal homogeneity ($\chi^2 = 9.976$, $p = 0.002$), as presented in Table 2. Additionally, restricted diffusion on MRI was significantly associated with the presence of peritumoral edema ($\chi^2 = 9.350$, $p = 0.002$), and a significant relationship was found between the presence of calcification on CT and bone changes such as hyperostosis or erosion ($\chi^2 = 19.959$, $p < 0.001$), as detailed in Table 3.

To assess the level of agreement between CT and MRI in evaluating tumor characteristics, Cohen's Kappa statistics were applied. The analysis revealed fair agreement across all three imaging features: tumor consistency ($\kappa = 0.318$), border definition ($\kappa = 0.376$), and signal homogeneity ($\kappa = 0.308$), as summarized in Table 4.

Table 2. Correlation of imaging features between CT and MRI Modalities Based on Chi-square Analysis (n = 100)

CT–MRI Comparative Features	χ^2 Value	df	p-value	Test Type	Significant ($p < 0.05$)
CT consistency vs. MRI consistency	10.526	1	**0.001**	Pearson chi-square	Yes
CT border vs. MRI border	30.483	4	**<0.001**	Pearson chi-square	Yes
CT homogeneity vs. MRI homogeneity	9.976	1	**0.002**	Pearson chi-square	Yes

Note. Abbreviations: χ^2 = Chi-square; df = degrees of freedom; $p < 0.05$ considered statistically significant.

Table 3. Diagnostic features association between diffusion restriction vs. peritumoral edema and calcification vs. bone changes in meningiomas (n = 100)

Diagnostic Feature Associations	χ^2 Value	df	p-value	Test Type	Significant ($p < 0.05$)
DWI Restriction vs. Peritumoral Edema	9.350	1	0.002	Pearson chi-square	Yes
CT calcification vs. bone changes	19.959	2	<0.001	Pearson chi-square	Yes

Note. Abbreviations: χ^2 = Chi-square; df = degrees of freedom; $p < 0.05$ considered statistically significant.

Table 4. Agreement between CT and MRI features in meningiomas using Cohen's Kappa coefficient. Interpretation was based on the Landis and Koch scale: $\kappa < 0.20$ (slight), 0.21–0.40 (fair), 0.41–0.60 (moderate), 0.61–0.80 (substantial), and >0.80 (almost perfect).

Imaging Features	CT Evaluation	MRI Evaluation	(κ)	Level of Agreement
Tumor Consistency	CT consistency	MRI-consistency	0.318	Fair
Border Definition	CT borders	MRI- borders	0.376	Fair
Signal Homogeneity	CT homogenity	MRI-homogeneity	0.308	Fair

Note. Abbreviations: κ = Cohen's Kappa; CT = Computed Tomography; MRI = Magnetic Resonance Imaging.

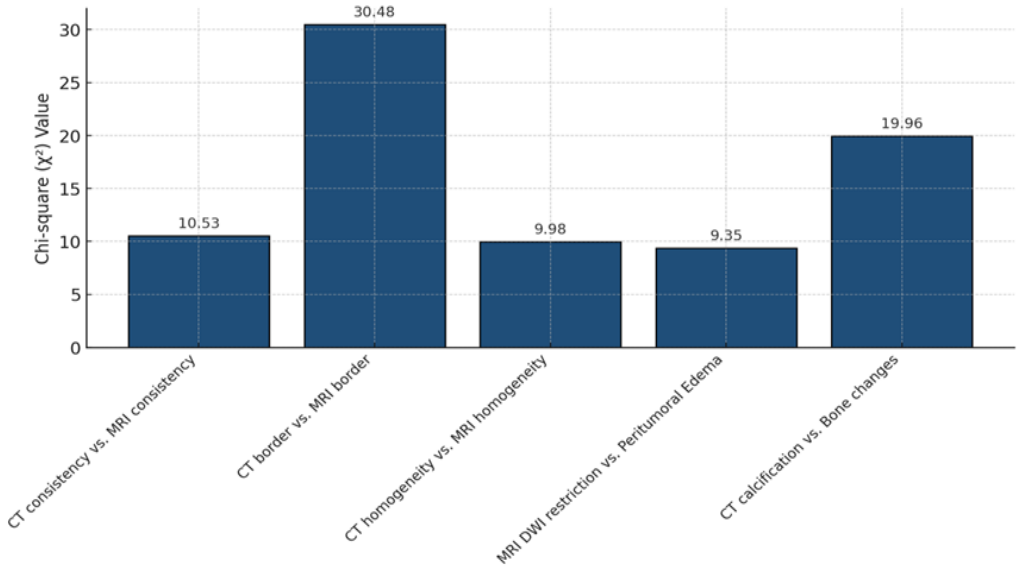

Figure 3. Column chart showing chi-square results of correlations and associations between key imaging features. The first three comparisons CT vs MRI consistency, border definition, and homogeneity represent cross-modality correlations. The final two comparisons, MRI DWI restriction vs. peritumoral edema and CT calcification vs. bone changes, demonstrate diagnostic feature associations within or across imaging modalities.

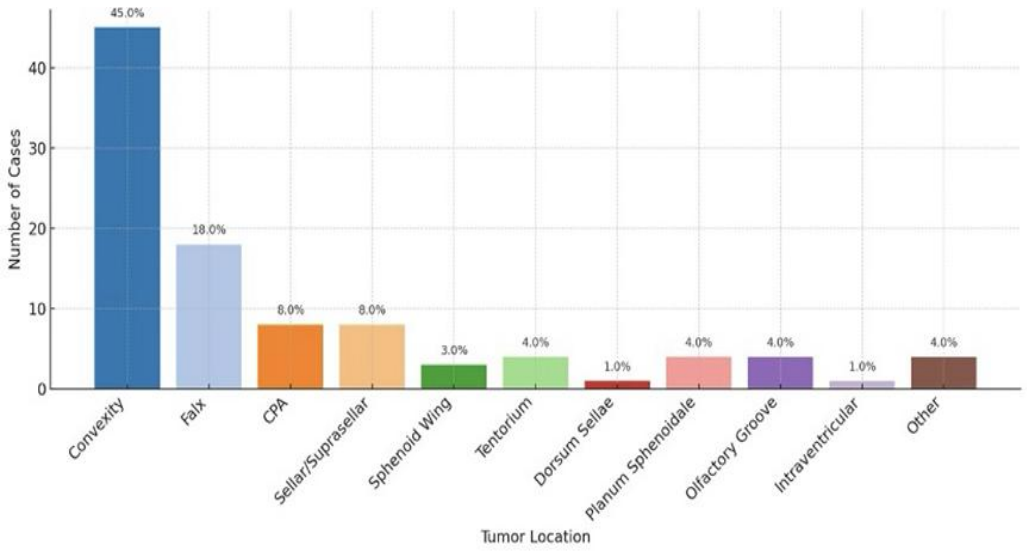

Figure 4. Column chart showing the distribution of tumor Locations among 100 patients with intracranial meningioma.

Note. Abbreviations: CPA= cerebellopontine angle

4. DISCUSSION

This study provides a comprehensive evaluation of intracranial meningiomas among Saudi patients to statistically examine correlations between CT and MRI features within the same cohort. The most frequent tumor sites in our cohort were the convexity (45%) and falx (18%) (Figure 4), consistent with reports by Nowosielski et al. and Varlotto et al., who identified these regions as the most common anatomical sites. Tumor location, particularly the distinction between skull base and non–skull base meningiomas, has important implications for surgical planning and operative risk. [1,7] Our findings also demonstrated a female predominance (72%) and peak incidence in the 51–60-year age group, aligning with Ostrom et al. and Ogasawara et al. and supporting the role of hormonal and age-related factors in meningioma development. [4, 8, 9]

A major strength of this study is the statistical demonstration of CT–MRI correlation for key radiologic features. Significant associations were observed between the two modalities for tumor consistency ($\chi^2 = 10.526$, $p = 0.001$), border definition ($\chi^2 = 30.483$, $p < 0.001$), and lesion homogeneity ($\chi^2 = 9.976$, $p = 0.002$) (Table 2). To our knowledge, this represents the first region-specific evidence systematically evaluating such relationships. Demonstrating correlation in these features is clinically relevant: tumor consistency influences resection difficulty, border definition reflects the likelihood of achieving complete removal, and homogeneity highlights intratumoral complexity. Establishing correlations between CT and MRI enhances diagnostic confidence and enables more reliable preoperative planning.

To further assess how consistently CT and MRI characterize the same features on a per-patient basis, Cohen's Kappa coefficient was applied. The analysis revealed fair agreement in tumor consistency ($\kappa = 0.318$), border definition ($\kappa = 0.376$), and signal homogeneity ($\kappa = 0.308$) (Table 4). These values suggest that, despite significant statistical association, the degree of concordance remains modest, reinforcing the complementary but not interchangeable nature of the two modalities. This highlights the importance of using both CT and MRI in combination to achieve a more comprehensive radiological assessment.

Most lesions in our study appeared hypointense to gray matter on T1-weighted MRI and hyperintense on T2-weighted sequences, consistent with Maiuri et al. and Gasparetto et al. Although many tumors were isointense on FLAIR, variability was noted, reflecting intratumoral heterogeneity and peritumoral edema. [6, 10, 11, 12]

A significant correlation between diffusion restriction and peritumoral edema ($\chi^2 = 9.350$, $p = 0.002$) (Table 3), further underscores the value of diffusion-weighted imaging (DWI). This finding is in line with Spille et al. and Ranabhat et al., who emphasized DWI's role in evaluating tumor cellularity and edema, both of which influence surgical complexity and patient outcomes. [2, 11, 12]

CT imaging proved indispensable in evaluating calcification and bone involvement. In this cohort, 47% of meningiomas demonstrated calcification and 26% showed hyperostosis, findings comparable to Zhao et al. Heterogeneous CT appearance was observed in 73% of cases, higher than the 18% reported by Hong et al., possibly reflecting greater prevalence of calcification, cystic change, or necrosis. We also identified a strong association between calcification and bone changes, including hyperostosis and erosion ($\chi^2 = 19.959$, $p < 0.001$) (Table 3), reinforcing CT's role in detecting subtle osseous alterations that are less apparent on MRI .[5, 13]

Together, these findings demonstrate that CT is essential for assessing calcification and bone changes such as hyperostosis, while MRI provides superior evaluation of soft tissue characteristics, intratumoral heterogeneity, and peritumoral edema. When interpreted in combination, these modalities allow anticipation of which tumors are more straightforward to remove and which may involve critical structures, such as the skull base or major vascular sinuses, thereby increasing surgical complexity or requiring earlier intervention. In addition, associated effects such as marked edema or mass effect , or ill-defined borders may prompt more urgent management. CT findings of hyperostosis or bony erosion are especially valuable when planning craniotomy size and surgical entry points .Recognizing these correlations preoperatively supports surgical planning , selection of operative technique and overall treatment decisions.

In our study, histopathological correlation was not available, and tumor consistency was therefore inferred from imaging alone. The study was conducted at a single center and was retrospective in nature. Finally, outcome data and long-term follow-up were not included, as the study was intentionally designed to focus on imaging features at the time of first diagnosis. Future multicenter studies incorporating histopathological correlation and clinical outcomes would help extend and build upon these results

5. CONCLUSION

This study provides a thorough evaluation of intracranial meningiomas among Saudi patients, encompassing demographic distribution, tumor location, and key imaging features on CT and MRI. In addition it demonstrated significant CT–MRI correlations and fair agreement in key imaging features, offering region-specific evidence that enhances diagnostic reliability. These findings underscore the value of a multimodal imaging approach in improving diagnostic confidence and optimizing preoperative planning.

6. CONFLICT OF INTEREST

The authors declare that they have no conflicts of interest related to this manuscript.

7. FUNDING

No funding was received to support this study

8. ACKNOWLEDGMENT

The authors would like to thank all individuals who contributed to the completion of this work. During the preparation of this manuscript, the authors used GPT-4 (OpenAI, San Francisco, USA) to enhance the readability of some sections, ensure consistency, and reduce redundancies. All content generated using this tool was carefully reviewed, edited, and approved by the authors, who take full responsibility for the final version of the manuscript.

9. REFERENCES

[1] Gasparetto EL, Leite CC, Lucato LT, Barros CV, Marie SKN, Santana P, et al. Intracranial meningiomas: magnetic resonance imaging findings in 78 cases. Arq Neuropsiquiatr. 2007;65(3A):610–4. doi:10.1590/S0004-282X2007000400012

[2] Hong KS, Choi SW, Kim SH, Kim HJ, Song JH, Choi JH. Are the clinical manifestations of CT scan and location associated with World Health Organization histopathological grades of meningioma? A retrospective study. Ann Med Surg (Lond). 2021; 66:102424. doi: 10.1016/j.amsu.2021.102424

[3] Huntoon K, Toland AMS, Dahiya S. Meningioma: A review of clinicopathological and molecular aspects. Front Oncol. 2020; 10:579599. doi:10.3389/fonc.2020.579599

[4] Louis DN, Ohgaki H, Wiestler OD, Cavenee WK, Burger PC, Jouvet A, et al. The 2007 WHO Classification of Tumors of the Central Nervous System. Acta Neuropathol. 2007;114(2):97–109. doi:10.1007/s00401-007-0243-4

[5] Maiuri F, Iaconetta G, de Divitiis O, Cirillo S, Di Salle F, De Caro ML. Intracranial meningiomas: correlations between MR imaging and histology. Eur J Radiol. 1999;31(1):69–75. doi:10.1016/S0720-048X(98)00083-7

[6] Nowosielski M, Galldiks N, Iglseder S, Kickingereder P, von Deimling A, Bendszus M, et al. Diagnostic challenges in meningioma. Neuro Oncol. 2017;19(12):1588–98. doi:10.1093/neuonc/nox101

[7] Ogasawara C, Philbrick BD, Adamson DC. Meningioma: A review of epidemiology, pathology, diagnosis, treatment, and future directions. Biomedicines. 2021;9(3):319. doi:10.3390/biomedicines9030319

[8] Ostrom QT, Gittleman H, Fulop J, Liu M, Blanda R, Kromer C, et al. CBTRUS statistical report: primary brain and central nervous system tumors diagnosed in the United States in 2008–2012. Neuro Oncol. 2015;17(Suppl 4): iv1–62. doi:10.1093/neuonc/nov189

[9] Ranabhat K, Bishokarma S, Agrawal P, Shrestha P, Panth R, Ghimire RK. Role of MR morphology and diffusion-weighted imaging in the evaluation of meningiomas: radio-pathologic correlation. JNMA J Nepal Med Assoc. 2019;57(215):37–44. doi:10.31729/jnma.4305

[10] Spille DC, Adeli A, Sporns PB, Heß K, Streckert EMS, Brokinkel C, et al. Predicting the risk of postoperative recurrence and high-grade histology in patients with intracranial meningiomas using routine preoperative MRI. Neurosurg Rev. 2020;44(2):1109–17. doi:10.1007/s10143-020-01301-7

[11] Varlotto J, Flickinger J, Pavelic MT, Specht CS, Sheehan JM, Timek DT, et al. Distinguishing grade I meningioma from higher grade meningiomas without biopsy. Oncotarget. 2015;6(35):38421–8. doi:10.18632/oncotarget.5376

[12] Zhang S, Chiang G, Knapp JM, Zecca CM, He D, Ramakrishna R, et al. Grading meningiomas utilizing multiparametric MRI with inclusion of susceptibility-weighted imaging and quantitative susceptibility mapping. J Neuroradiol. 2020;47(4):272–7. doi:10.1016/j.neurad.2019.05.002

[13] Zhao X, Yu RT, Li JS, Xu K, Li X. Clinical value of multi-slice 3-dimensional computed tomographic angiography in the preoperative assessment of meningioma. Exp Ther Med. 2013;6(2):475–8. doi:10.3892/etm.2013.1147